Title 1

Design, Control, and Clinical Implementation of an Open Source Bionic Leg 2

3 Authors

- Alejandro F. Azocar^{1,2}, Luke M. Mooney³, Jean-François Duval³, Ann M. Simon^{4,5}, Levi J. Hargrove^{4,5,6}, 4
- Elliott J. Rouse^{1,2}* 5

6 **Affiliations**

- ¹Department of Mechanical Engineering, University of Michigan, Ann Arbor, MI 48109 USA. 7
- 8 ²Robotics Institute, University of Michigan, Ann Arbor, MI 48109 USA.
- 9 ³Dephy, Inc., Maynard, MA 01754 USA.
- ⁴Center for Bionic Medicine, Shirley Ryan AbilityLab, Chicago, IL 60610 USA. 10
- ⁵Department of Physical Medicine and Rehabilitation, Northwestern University, Chicago, IL 60611 USA. 11
- 12 ⁶Department of Biomedical Engineering, Northwestern University, Evanston, IL 60208 USA.
- *Corresponding author. Email: ejrouse@umich.edu 13

14 **Abstract**

- Today's passive prosthetic technologies limit the well-being of millions of individuals with amputations, who 15
- 16 often walk slower, use more energy, fall more often, and develop devastating secondary deficits over time.
- Robotic prostheses hold the promise to address many of these challenges, but safe, reliable control strategies 17
- have remained out of reach—that is, a critical gap is the ability to provide appropriate instructions to robotic 18
- legs that enable robust ambulation in the real world. Fortunately, there are many researchers studying control 19
- strategies, but each group tests their strategies with different robotic hardware in constrained laboratory 20
- settings. This mismatch in prosthesis hardware severely limits comparison of control solutions and, along with
- 21
- 22 the lack of testing in real-world environments, hinders the translation of these promising technologies. To
- address these challenges, we developed the Open Source Leg (OSL): a robotic knee-ankle prosthesis that 23
- facilitates controls, biomechanics, and clinical research. This paper describes the design innovations required 24
- to develop a bionic leg for broad dissemination, characterization of the OSL's electromechanical performance, 25
- and clinical demonstration with an advanced high-level control strategy, tested with three individuals with 26
- above-knee amputations. The OSL provides a common hardware platform for scientific studies and clinical 27
- testing, lowers the barrier for new prosthetics research, and enables research beyond the laboratory; in more 28
- 29 realistic environments, such as the hospital, community, and home.

Introduction

31

43

44

45

46

47

48

49

50

51

52

53

54

55

56

57

58

59

60

61

62

63

64

65

66

67

68

69

70

71

72

73

74

Millions of people with lower-limb amputations suffer from a reduced quality of life^{1,2}. Physically, the 32 majority of these individuals walk slower, get tired faster, and are less stable than non-amputees, partly due to 33 the passive nature of traditional prosthetic legs³⁻⁵. In the intact human body, leg muscles contract during 34 walking to add mechanical energy⁶; however, passive prostheses are not able to provide this energy, and, 35 subsequently, cannot restore the natural functions of muscles lost during an amoutation. This makes more 36 37 demanding activities, such as climbing stairs and ramps, particularly difficult⁷. Additionally, individuals with lower-limb amputations often develop compensatory modifications to their gait, biomechanics, and muscle 38 activation patterns that lead to further complications, such as osteoarthritis, osteoporosis, and back pain^{8–10}. 39 Finally, the resulting mobility challenges can lead to depression, social stigmatization, and 40 unemployment^{2,11,12}. Although passive prostheses provide substantial mobility benefits, their physical, 41 psychological, and social impacts limit the quality of life for many individuals with amputations. 42

Several research groups are developing powered knee, ankle, and knee-ankle (whole-leg) prostheses that have the potential to address many of the challenges stemming from their passive counterparts^{13–21}. Powered prostheses typically use electric motors that are able to add net-positive mechanical energy similar to the muscles within the leg. Powered knee prostheses include the Clutchable Series-Elastic Actuator (CSEA) and the ANGle-dependent ELAstic Actuator (ANGELAA) knees^{22,23}; the CSEA Knee is capable of recreating early-stance knee flexion and extension—a region of the gait cycle that most passive prostheses cannot reproduce safely^{24,25}. Previously developed powered ankle prostheses include the MIT Powered Ankle-foot Prosthesis, SPring Ankle with Regenerative Kinetics (SPARKy), Ankle Mimicking Prosthetic (AMP) Foot, and the Robotic Transtibial Prosthesis (RoboTPro)²⁶⁻²⁹; compared to passive prostheses, amputees using powered ankles walk faster, use less energy, and/or exhibit improved center of pressure progression, although there has been debate on the applicability of these systems for people with lower activity levels³⁰. Powered knee-ankle systems include the Vanderbilt Powered Leg (VPL) Prosthesis and the University of Utah Lightweight Leg^{31–33}; these prostheses combine the benefits of powered knee and ankle prostheses. Finally, prosthesis emulators are a recently-developed alternative for quickly and systematically testing control systems^{34,35}. Emulators utilize off-board motors and Bowden cable tethers, leading to high performance and low prosthesis weight; however, the tether between the motor and prosthesis can limit experiments to a laboratory setting with a treadmill.

There have also been promising advances in the development of safe, natural, and intuitive control approaches. Today's state-of-the-art control architectures typically include three overarching levels of control, each bearing responsibility for certain aspects of successful community ambulation. The control systems must recognize the user's intended movement (*i.e.*, high-level control), translate the intended movement into an appropriate pattern of leg movement and effort (mid-level control), and execute the desired motions with closed-loop control (low-level control)³⁶. Errors or failures at any of these levels may lead to falls, injuries, loss of confidence, and reduced community mobility. Fortunately, this is an active area of research, with many groups studying different approaches. For example, existing mid-level strategies implement impedance-based control, phase-based control, or biologically-inspired neuromuscular models^{16–18,31}. High-level control approaches use simple thresholds or implement machine learning techniques to automatically transition between mid-level control strategies for different ambulation modes, such as level ground walking, ramp ascent/descent, and stair ascent/descent^{31,37}. Overall, control systems for robotic legs are highly sophisticated—sometimes containing over 100 parameters, requiring multiple hours of tuning³⁸. Thus, despite promising work, key challenges remain in the development of control strategies that are safe, robust, and intuitive.

Although talented researchers around the world are investigating the best ways to control robotic prostheses, development of prosthetic hardware requires substantial investments of time and resources before research can begin. Even after research is complete, differences in design, performance, and limitations hinder the ability to compare the merits of different control systems. For example, robotic prostheses today vary widely in size, weight, transmission type, controllability, and degrees of freedom; additionally, many research prostheses must be tethered to a power supply—preventing researchers from testing in more challenging and realistic environments. Finally, since most research prostheses are prototypes, they are typically only tested in a few studies by the original designers, and can be difficult for other researchers to use. The lack of a low-cost, high-performance, and accessible powered prosthetic leg technology has hindered progress in the field, and ultimately, the quality of life of individuals with lower-limb amputations.

To facilitate the study and fair comparison of control approaches, lower the barrier to performing controls research, and prevent duplication of effort, we have created the Open Source Leg (OSL): a unique robotic knee-ankle prosthesis system developed for open-source dissemination (Fig. 1). The OSL includes novel prosthesis hardware, actuation, sensing, low-level control software, and software libraries to communicate with researcher-specific mid- and high-level control systems. In this article, we present the design, technical characteristics, and performance of the OSL. We provide a detailed description of the design process, mechatronics implementation, benchtop testing, and highlight two novel design components—implementation of high-torque motors and an easily-modifiable series-elastic actuator. Finally, we demonstrate individuals with amputations successfully walking with the OSL across level ground, ramps, and stairs with an existing high- and mid-level control strategy, with all control parameters provided for reference for future researchers³⁸.

Results

Design overview. The OSL incorporates a number of design innovations to facilitate dissemination and high performance. For example, we used electric motors that were originally developed by the drone industry, and are rarely used in wearable robotic applications³⁹ (Fig. 1, Table S1). These motors produce 2-10 times more torque than the motors typically implemented in prosthetic legs, allowing us to implement transmission ratios 2-5 times lower than comparable prostheses (Table 1). Transmissions amplify the torque produced by the motors, and low transmission ratios are important in prostheses because they improve size, electrical power demands, bandwidth, and audible noise, ultimately impacting mass, battery size, controllability, and other factors. Additionally, the OSL incorporates selectable series elasticity: the knee functions either as a serieselastic actuator (SEA)—and allows for modification of the series stiffness—or as a non-SEA (Fig. 1)⁴⁰. Selectable series elasticity allows researchers to use the SEA for energy storage/return, shock tolerance, and torque control, whereas the non-SEA is simpler, lighter, and requires motor current to estimate torque. Depending on the desired magnitude of the series stiffness element, up to six springs disks—each with a stiffness and mass of 97 ± 20 Nm/rad and 23 g, respectively—can be stacked inside the knee's transmission, resulting in a compact SEA without any added volume (Fig. 1). Finally, the OSL (4 kg) is 20% lighter than similar prostheses and is fully self-contained—including batteries (36 V/950 mAh), sensing, and computation—two key characteristics for portability and testing outside of laboratory conditions (Table 1).

We included embedded electronic systems that handle sensing, low-level control, and communication, enabling researchers to focus on clinical testing and novel higher level control strategies. The OSL is powered by the Dephy Actuator Package (DAP), which integrates the high torque motor with a commercialized version of the Flexible Scalable Electronics Architecture (FlexSEA) in a compact, reliable platform^{41,42} (Fig. 1). The DAP implements low-level motor control and field oriented control commutation; closes the feedback loops in the position, velocity, current, and impedance controllers; and facilitates communication between the motor controller and external computers/sensors, via Universal Serial Bus (USB), Bluetooth, Serial Peripheral Interface (SPI), Inter-Integrated Circuit (I²C), RS-485, or Universal Asynchronous Receiver/Transmitter (UART) protocols. To control overall prosthesis behavior, researchers provide mid- (e.g., desired position, desired current, controller gains, etc.) and high-level (e.g., ambulation mode, state, etc.) control commands, using their preferred embedded hardware system (e.g., single-board computer, laptop computer) and an open-source Python or MATLAB Application Peripheral Interface (API) (Fig. 2). A graphical user interface (GUI) is

125 also
126 DAI
127 mea
128 can l
129 inclu
130 prote
131

also available to quickly test the system, tune controllers, and display and save sensor data. The OSL and DAP include the following sensors: winding and bus electrical states, temperature, nine-axis inertial measurement unit (IMU), a 14-bit motor encoder, and a 14-bit joint encoder (Table S1). A six-axis load cell can be mounted to either the knee's distal or the ankle's proximal pyramid adaptor (Fig. 1). Finally, the DAPs include a number of features to improve safety and reduce user error, including: over- and under-voltage protection, over-current protection with programmable and physical fuses, and electrostatic discharge protection on the inputs and outputs.

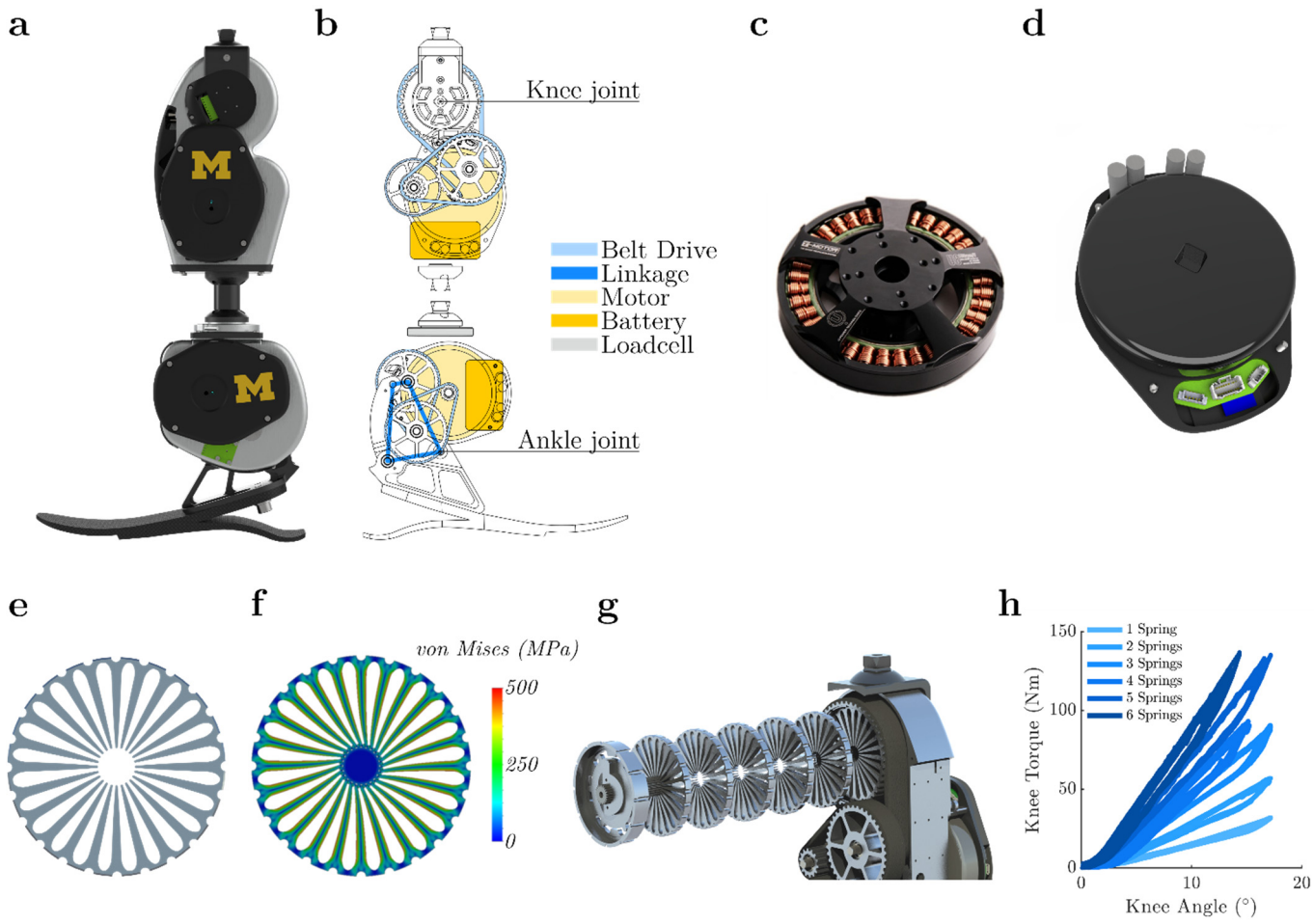


Figure 1 | **The Open Source Leg (OSL) and its novel design components. a**, Rendering of the OSL. **b**, Schematic of the OSL highlighting the transmission, electronics, and loadcell. **c**, Output view of the electric motor used in the OSL. **d**, Output view of the Dephy Actuator Package (DAP), which includes the electric motor and accompanying electronics. **e**, Side view of a single spring disk. **f**, Finite element analysis of a spring disk being deflected by the gear-shaped internal shaft. Colors represent the von Mises stress. **g**, Exploded view of six springs stacked inside the knee output pulley. **h**, Torque-angle relationship of the knee with 1-6 springs stacked inside. Each spring has a stiffness of approximately 100 Nm/rad.

152

153

154

156

157

158

159

160

161

Table 1. OSL specifications with comparison to other prostheses and the human body.

		OSL	MIT	Vanderbilt	Utah	Human ^g
Mass	Knee	2160-2330 ^a	2700	2700 ^d	1680	2616 ^h
(g)	Ankle	1740	2000	2300	1045 ^e	1959 ⁱ
Height	Knee	240	285		290	314 ^h
(mm)	Ankle	213	220	210	120	$171^{\rm i}$
Range of Motion	Knee	120	120	120	120	90
(°)	Ankle	30	45	65	55	60
Tourseissien Detie	Knee	49	143	176	0-375	-
Transmission Ratio	Ankle	58 ± 16^{b}	170	116	50-800	-
Series Elasticity	Knee	100-600	240	- -	-	-
(Nm/rad)	Ankle	-	1688^{d}	-	-	-
Peak Torque,	Knee	50°	40	-	-	-
Continuous (Nm)	Ankle	59 ± 16^{c}	-	-	-	-
Peak Torque,	Knee	150°	120	85	125	90
Instantaneous (Nm)	Ankle	178 ± 49^{c}	125	150	125	105
Peak Speed	Knee	5.2	-	-	-	6.8
(rad/s)	Ankle	5.6	-	-	-	5.4
Position Bandwidth	Knee	10-20	-	-	$7^{\rm f}$	2^{j}
(Hz)	Ankle	10-20	-	-	-	4 ^j
Torque Constant	Knee	0.14	0.028	0.028	0.014	-
(Nm/A)	Ankle	0.14	0.060	0.053	0.014	<u>-</u>
Motor Constant	Knee	0.182	0.044	0.044	0.023	-
$(Nm/W^{1/2})$	Ankle	0.182	0.057	0.096	0.043	<u>-</u>
Bus Voltage	Knee	36	24	24	24	-
(V)	Ankle	36	24	24	24	_

- Not applicable/available
- a Knee mass varies with SEA configuration
- b See Fig. S5for ankle transmission ratio profile
- c Estimated with torque constant, transmission ratio, continuous (10 A) and instantaneous (30 A) motor current, and 90% efficiency at each transmission stage
- d Estimated
- e Does not include batteries or electronics
- f 10° amplitude
- g Assuming a 75 kg, 1.7 m tall subject walking on level ground or ascending/descending stairs
- h Assuming 75% shank mass and height
- i Assuming 25% shank plus foot mass and height
- j Defined as the frequency range over which 70% of the total signal power is captured

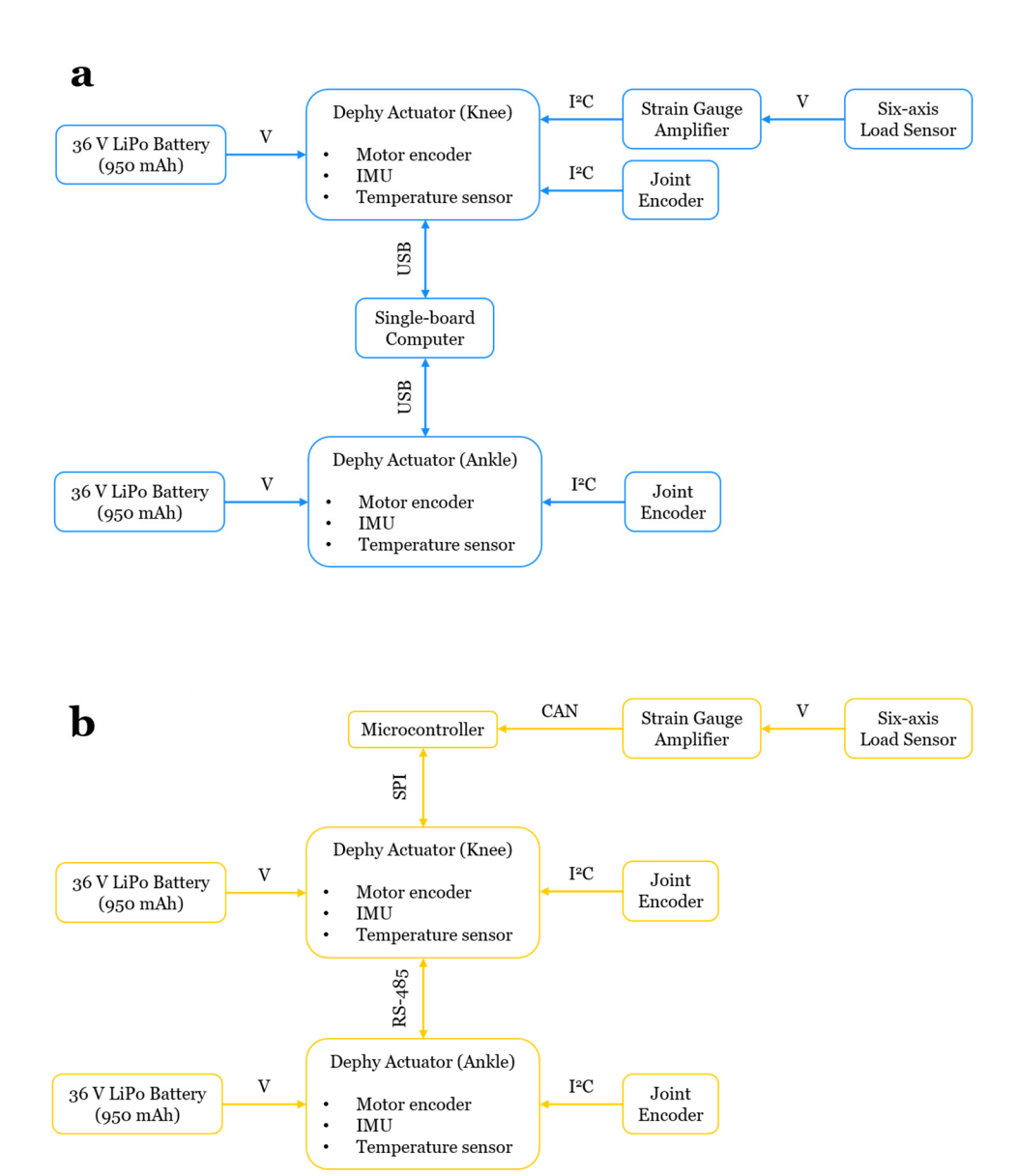


Figure 2 | Two possible embedded system configurations. High-level overview of electronics, sensors, and power supplies, along with the type of communication between components. **a**, The DAPs are connected in parallel with a single-board computer via USB; this configuration was used for the benchtop testing, with a single motor. **b**, The DAPs are connected in series with a microcontroller, and the load sensor communicates with the microcontroller via Controller Area Network (CAN) bus; this configurations was used for the clinical testing.

Benchtop testing. To facilitate the success of future researchers who may use the OSL, we completed electromechanical and thermal performance testing using a benchtop setup. We tested the low-level position and current controllers in the time and frequency domains, and also tracked the OSL's temperature increase during 70 minutes of continuous operation.

A step response test was used to quantify the OSL's ability to track changes in desired position and current reference values; frequency response tests estimated the bandwidth—the range of input frequencies that the OSL can track with high fidelity—of the low-level position and current controllers. Motor current is often used in prostheses to estimate output torque, and the current controller's performance is critical for open-loop torque and impedance control. The position and current controllers exhibit fast and accurate step responses,

with bandwidths of 10.7-20.2 Hz and >200 Hz, respectively (Fig. 3, Table 1). In approximately 30% of the current bandwidth trials, the magnitude of the frequency response did not fall below -3 dB within the measured frequency range, indicating that bandwidth was higher than the Nyquist frequency (375 Hz). Further results on the controller performance can be found in our previous work⁴³.

The heat generated by an electric motor (equation (7)) ultimately limits the torque it can generate, and how long it will operate safely. Therefore, we quantified the thermal response, and developed a thermal model of the motor and OSL to a current step input of 8 A direct current (DC) (Fig. 3, Movie S1); the current was supplied across two winding leads, which is equivalent to approximately 6.5 A of torque producing DC current for a delta-wound motor (*i.e. q*-axis current), producing approximately 12 W of thermal heat flux. Starting from an ambient temperature of 25 °C, the T-motor windings reached a steady-state temperature of 92 °C; when the DAP electronics plate—which acts as an additional heatsink—was included, the windings and housing (plate) reached steady-state temperatures of 83 °C and 64 °C, respectively. From the experimental data, we calculated the motor's thermal resistance and capacitance and simulated the motor's thermal response (Fig. 3). Our simulation predicts that the motor can operate at its continuous (10 A *q*-axis) and peak (30 A *q*-axis) current limits—corresponding to approximately 50 Nm and 150 Nm of joint torque (Table 1)—for 513 s and 17 s, respectively, before reaching unsafe temperatures (set at 125 °C). In these simulations and the paper as a whole, the current reported is the *q*-axis current, which is analogous to the DC current in the standard brushed electromechanical model⁴⁴.

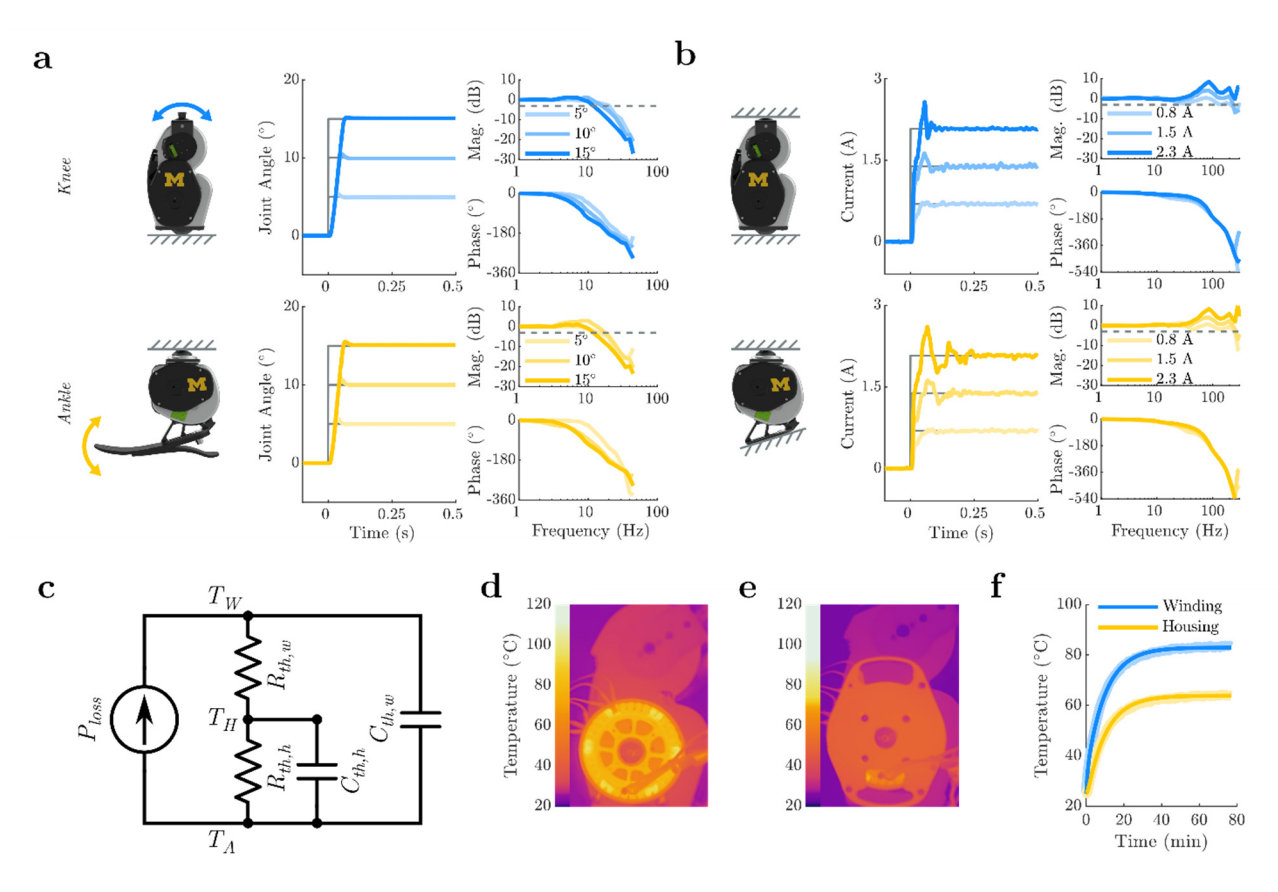


Figure 3 | **Electromechanical and thermal benchtop testing. a**, Test setup, step response, and frequency response for the position control system. The output of each joint was free to rotate for these tests. The dashed line represents the -3 dB threshold used to calculate bandwidth. **b**, Test setup, step response, and frequency response for the current control system. The output of each joint was locked in place for these tests. **c**, Equivalent electrical circuit used to model the thermal dynamics of the motor. **d**, Thermal image of the knee prosthesis, without the DAP electronics plate, after providing the motor with a constant current of 8 A DC across two winding leads for 70 minutes. **e**, Thermal image of

the knee prosthesis, with the DAP electronics plate, after providing the motor with a constant current of 8 A DC for 70 minutes. **f**, Simulated (bold) and experimental (shaded) thermal response of the motor to a constant current of 8 A across two leads.

Clinical testing. The OSL was tested clinically to demonstrate efficacy, as well as provide details of an existing high and mid-level controller that produces known gait patterns and biomechanical data. The intent of these data is to serve as a benchmark for future researchers developing new control strategies. Thus, we conducted clinical testing with three individuals with unilateral transfemoral (above-knee) amputations (Table S2, Fig. 4) who did not have prior experience with the OSL, but did have prior experience ambulating with the VPL Prosthesis³¹. We implemented an impedance-based control system to enable meaningful ambulation modes at a rehabilitation hospital³⁸. Each subject provided written informed consent, approved by the Northwestern University Institutional Review Board. Testing occurred across two separate visits.

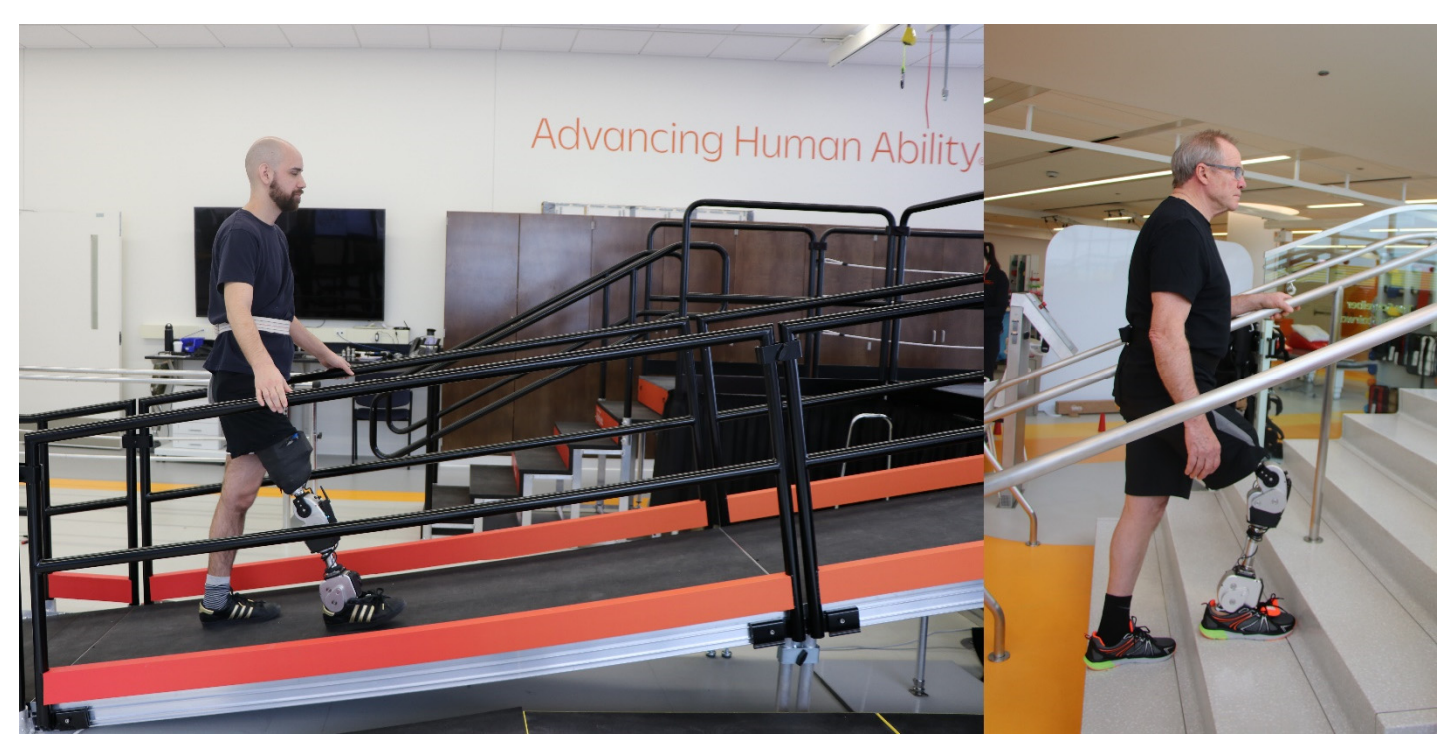


Figure 4 | Subjects with a transfemoral amputation ambulating with the OSL.

During the first visit, a certified prosthetist fitted and aligned the OSL to each subject, ensuring suspension, comfort, and stability on the leg during standing. Next, subjects walked within a set of parallel bars while we tuned the impedance parameters for level-ground walking. Subjects subsequently ambulated up/down stairs, and up/down ramps while we tuned the impedance parameters using a combination of visual inspection and feedback from the prosthetist, a physical therapist, and the subjects (Fig. 5); tuning continued until a set of clinical ambulation goals—including appropriate weight acceptance, plantarflexion, knee power, swing clearance, step length, walking speed, and minimal upper extremity support—were met, and the prosthetist, therapist, and subjects were satisfied with the OSL's performance³⁸. This visit lasted approximately 2-3 hours.

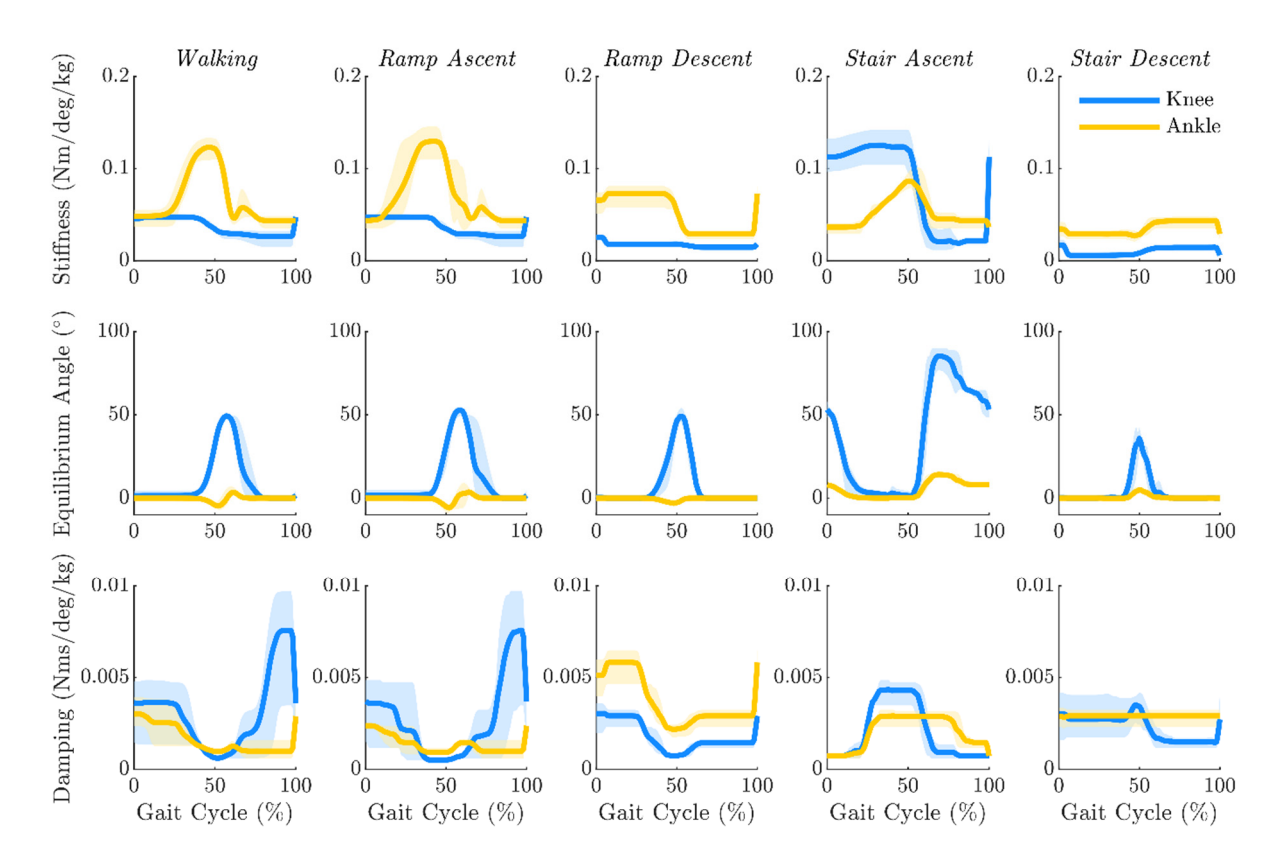


Figure 5 | **Tuned impedance parameters across five ambulation modes.** Mean (bold) and range (shaded) of virtual stiffness, equilibrium angle, and damping coefficient profiles for 3 subjects, tuned for level ground, ramp ascent/descent, and stair ascent/descent.

During the second visit, subjects performed a series of ambulation circuits that included all of the following activities: standing, walking, stair ascent, stair descent, ramp ascent, and ramp descent, as described in prior work^{37,45}. The circuit included seamless transitions between activities, achieved using a mobile phone that communicated with the embedded controller⁴⁶. Seamless transitions within the experiment included: standing to walking, walking to standing, walking/standing to stairs, stairs to walking/standing, walking to ramps, and ramps to walking. We instructed subjects to ambulate at a comfortable speed and recorded data using the OSL's on-board sensors. This visit also lasted approximately 2-3 hours.

The subjects in this study exhibited similar joint kinematics and kinetics to those from our previous work (Fig. 6)³⁸. While walking on level ground and ramps, subjects achieved plantarflexion during early stance, controlled dorsiflexion during mid-stance, and powered push-off in late stance. Subjects successfully descended ramps and stairs with a reciprocal gait pattern by taking advantage of stance-phase knee flexion; during stair ascent with a reciprocal gait, subjects relied primarily on knee extension to propel themselves up and forward. Across all ambulation modes, peak knee flexion angles agreed to within 1-31% of able-bodied knee flexion and vertical ground reaction forces (GRFs) agreed to within 2-42% of able-bodied GRFs; for level-ground and ramp ambulation, peak ankle torques agreed to within 2-44% of able-bodied ankle torque. Subjectively, subjects noted during ambulation that the leg felt supportive, responsive, and smooth.

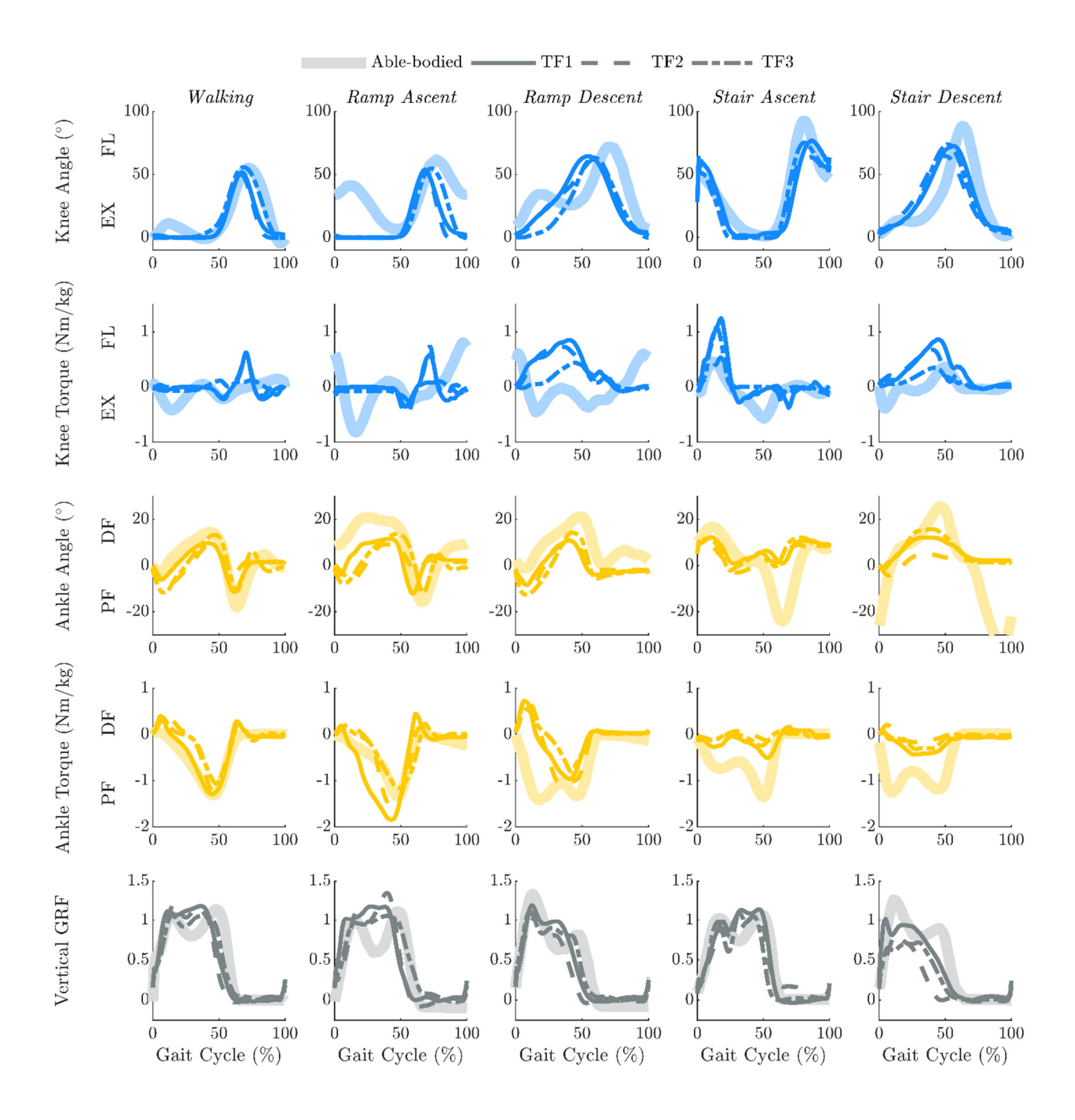


Figure 6 | OSL kinematics and kinetics across five ambulation modes. Mean user and able-bodied joint angles, moments, and vertical GRFs for level ground, ramp ascent/descent, and stair ascent/descent. Joint torques are normalized by subject mass and GRF is normalized by subject weight.

Discussion

This study describes the design, implementation, and characterization of an open-source robotic knee-ankle prosthesis, and demonstrates control with three subjects with transfemoral amputations successfully ambulating with the leg on level ground, ramps, and stairs. The OSL is intended to be a simple, portable, scalable, customizable, and economical hardware platform for development and evaluation of control systems, both in and out of the laboratory (Fig. 1).

Design. The intent of our design was to provide the highest performance, while facilitating ease-of-use, as well as reducing mass and cost. We implemented brushless electric motors from the drone industry because their efficiency and torque density permitted lower transmission ratios, enabling the use of timing belt drive transmissions, instead of more expensive or complex alternatives that can have substantial product lead times and cost (*e.g.*, harmonic drives, roller screw transmissions) (Fig. 1). Additionally, the integration of Dephy actuation technology allows researchers to focus on mid- and high-level control strategies, rather than developing low-level controllers and communication protocols. The DAPs and the associated Python, MATLAB, and C/C++ APIs lower the barrier to using the OSL. The Dephy technology embeds electrical and temperature sensors, an IMU, and a motor encoder; provides simple position, current, and impedance controllers; and automatically implements I²C, SPI, USB, RS-485, UART, and Bluetooth communication (Fig. 2).

The OSL's low mass and compact power supply enable research beyond typical lab-based treadmill tests. The OSL is shorter than the 4th percentile and lighter than the 16th percentile male shank and foot^{6,47}. The housings completely encompass the transmissions, batteries, and most of the electronics, reducing the risk of contamination or injury. Finally, the knee and ankle have independent embedded control hardware and batteries, allowing researchers to work with either the entire leg or a single joint. The portability and scalability of the OSL provide the capability to test control laws with both above- and below-knee amputees in indoor and outdoor environments.

The customization options enable the OSL to be suited to the individual uses of each researcher. The knee functions either as an SEA or non-SEA, and the stiffness magnitude of the series elasticity can be selected by the researcher. The springs fit inside of the belt drive's output pulley; therefore, the SEA configuration does not change the OSL's volume (Fig. 1). Although the ankle does not include a specific series elastic element, it can integrate with either a compliant commercial foot or a rigid flat foot. In addition to hardware customization, researchers have multiple options for high-level control implementation. For example, we used two different embedded computers (Raspberry Pi 3 vs. Texas Instruments DM3730) and communication protocols (USB vs. SPI) to control the motors in the benchtop and clinical tests (Fig. 2). The OSL also functions with other high-level control schemes (*e.g.*, MATLAB/Simulink, Robot Operating System, *etc.*) and external sensors (*e.g.*, electromyography, additional IMUs, *etc.*).

Clinical testing. All subjects in this study successfully ambulated on level ground, ramps, and stairs using the OSL, with all control parameter trajectories provided for reference (Fig. 4-6). Across most ambulation modes, joint angle and torque trajectories followed similar timing and amplitude patterns to able-bodied data⁴⁸⁻⁵⁰; however, there are notable differences. For example, subjects did not demonstrate early-stance knee flexion during level ground walking (Fig. 6). At heel contact, transfemoral amputees often pull back with their hip extensors to lock their prescribed, passive knee prosthesis into knee extension to prevent buckling and injury from falling; due to this habit, the subjects overrode the impedance controller's natural dynamics in favor of an extended knee joint. Additionally, subjects relied primarily on the knee to ambulate up and down stairs; the ankle provided little torque and only rotated through approximately 30% of its range of motion. It is important to note that the OSL is capable of producing early-stance knee flexion and ankle power across all ambulation modes; however, the subjects exhibited compensatory movement based on their daily ambulation strategies with a passive prosthesis. We can overcome these compensatory motions through training (not shown), or by tuning the controller to recreate able-bodied kinematics and kinetics; however, that was not the goal of this demonstration. We chose to not train the patients to overcome their compensatory strategies because they needed to return to their daily-use prosthesis after the experiment; we had concerns that such training on the OSL might lead to a fall when they returned to their daily-use device, which did require compensatory strategies. Instead, we tuned the OSL to meet a set of clinical ambulation goals. Overall, our implementation succeeded in performing similarly to walking with the VPL Prosthesis using the same impedance controller³⁸.

The OSL is capable of locomotion for extended periods of time. During level ground walking, the knee and ankle operate at 9.3 and 11.2 W, respectively, and the electronics operate at approximately 1 W. Given the energy in the batteries (34.2 Wh), a user could walk continuously for approximately 2.8 hours, 13.1 km, or 8,750 strides (i.e., 17,500 total steps) on a single charge, assuming consistent power consumption, a walking speed of 1.3 m/s, and cadence of 104 steps/min²². The batteries lasted for the entire duration of our experiments (3 hours). On average, lower-limb amputees walk approximately 6,000 steps/day, and healthy able-bodied adults are considered active if they walk at least 10,000 steps/day^{51,52}. Therefore, the OSL batteries have sufficient capacity for lab sessions and daily ambulation.

Benchmarks and limitations. Prosthesis mass and size play a critical role in the success of prosthetic legs. Heavy prostheses require higher metabolic expenditure from the user⁵³; this effect increases as the mass moves distally (*i.e.*, towards the ankle). Additionally, as the build height of a prosthesis increases, fewer users can wear the leg; that is, if the prosthesis is too long, it will not fit below the residual limb. Therefore, it is critical to design lightweight and short prostheses. The OSL (~4000 g) is approximately 20% lighter than comparable prostheses, with the exception of the Utah Lightweight Leg^{32,33} (~2800 g) (Table 1). The minimum build height of the OSL (~450 mm) is also comparable to the build height of other prostheses. Finally, the OSL is lighter and shorter than the foot and shank of a 75 kg, 1.7m tall adult (Table 1).

A limitation of the OSL is the ankle joint's range of motion (Table 1). During most ambulation tasks, the biological ankle remains within 10° of dorsiflexion and 20° of plantarflexion, as in the OSL; however, some subjects require a range of motion of 45-60° during stair descent^{48,50}. Many other prosthetic ankles have a range of motion of 45-65°. The OSL ankle's 30° range of motion is limited by the kinematics of the four-bar linkage, and could be improved by decreasing the ankle's transmission ratio or using a different transmission design (Fig. S1). However, amputees with passive prostheses can typically only achieve 10-15° during stair descent⁵⁴; therefore, although the OSL ankle does not achieve the full biological range of motion, it provides a substantial improvement over passive prostheses. The OSL knee's range of motion is equal to other prostheses (120°), and is much higher than needed for typical ambulation tasks (70-90°) (Table 1).

Transmission ratios determine prosthesis size, electrical demands, efficiency, performance, and other factors. Using the high-torque drone motors, we reduced transmission ratios to 2-5 times lower than comparable prostheses (Table 1). The combination of high-torque motors and low transmission ratios enables the OSL to produce peak torques similar to other systems, while demonstrating higher bandwidth. For example, the OSL's position bandwidth is approximately 5 times higher than the bandwidth of the biological knee or ankle; that is, the OSL is capable of recreating the human kinematics and kinetics (Table 1). The motors on the OSL have an overall winding-ambient thermal resistance of 3.9 K/W, compared to the 7.6 K/W thermal resistance of motors used in the CSEA Knee and VPL Prosthesis. In addition to being 1.3-2 times more electrically efficient than the CSEA and VPL knees, the OSL's motors produce 2.5-4 times less heat at steady-state, for a given joint torque (Fig. S2).

Summary and dissemination. In this paper, we present the design and mechanical, electrical, and thermal evaluation of an open-source robotic knee-ankle prosthesis, and demonstrate subjects walking with it across a range of activities, while providing controller parameters for reference. Future work includes advancement of the embedded systems, using the SEA for closed-loop torque control, and development of bio-inspired impedance control policies.

Researchers have access to the OSL through our companion website: www.opensourceleg.com. The website includes solid model files, a bill of materials, links to suppliers, control system code, instructional guides, videos on assembly/disassembly, and any other relevant information to improve the usability of the OSL. Furthermore, we have developed an online forum to allow researchers to post questions, results, or

independently developed modifications. We will also produce an open-source version of our high-level

controller that runs on a desktop or mobile device, providing researchers with a simple method of manually/automatically switching between ambulation modes and testing in non-steady-state conditions. Together, these tools will help researchers use the OSL and encourage a more collaborative community focused on transforming amputee quality of life.

Materials and Methods

Design: overview. To ensure that the OSL is accessible by researchers from diverse backgrounds (*e.g.*, controls, biomechanics, clinical, *etc.*), we abided by the following design principles:

- 1. *Simple*: the OSL does not use any precision machine components and can be assembled and disassembled with relative ease.
- 2. *Portable*: the OSL weighs less than the biological counterpart, and each joint has an on-board battery, facilitating research outside of the laboratory.
- 3. *Scalable*: the knee and ankle joints can operate independently, enabling research with both above-and below-knee amputees.
- 4. *Customizable*: a number of features in the leg hardware are customizable, and may be needed by certain researchers, depending on type of study.
- 5. *Economical*: the OSL costs approximately \$10,000-\$30,000 in prototype quantities, depending on degrees of freedom and sensing options, given today's manufacturing and material costs.

We designed the OSL through a multi-step design process which involved modeling human joint biomechanics, transmission kinematics, mechatronics (including motor electrical and thermal limitations), and the structural housing (Fig. 7). This was an iterative design process with the overall goal of achieving ablebodied kinematics/kinetics while meeting the desired design principles, minimizing prosthesis mass/volume, and satisfying mechatronic constraints.

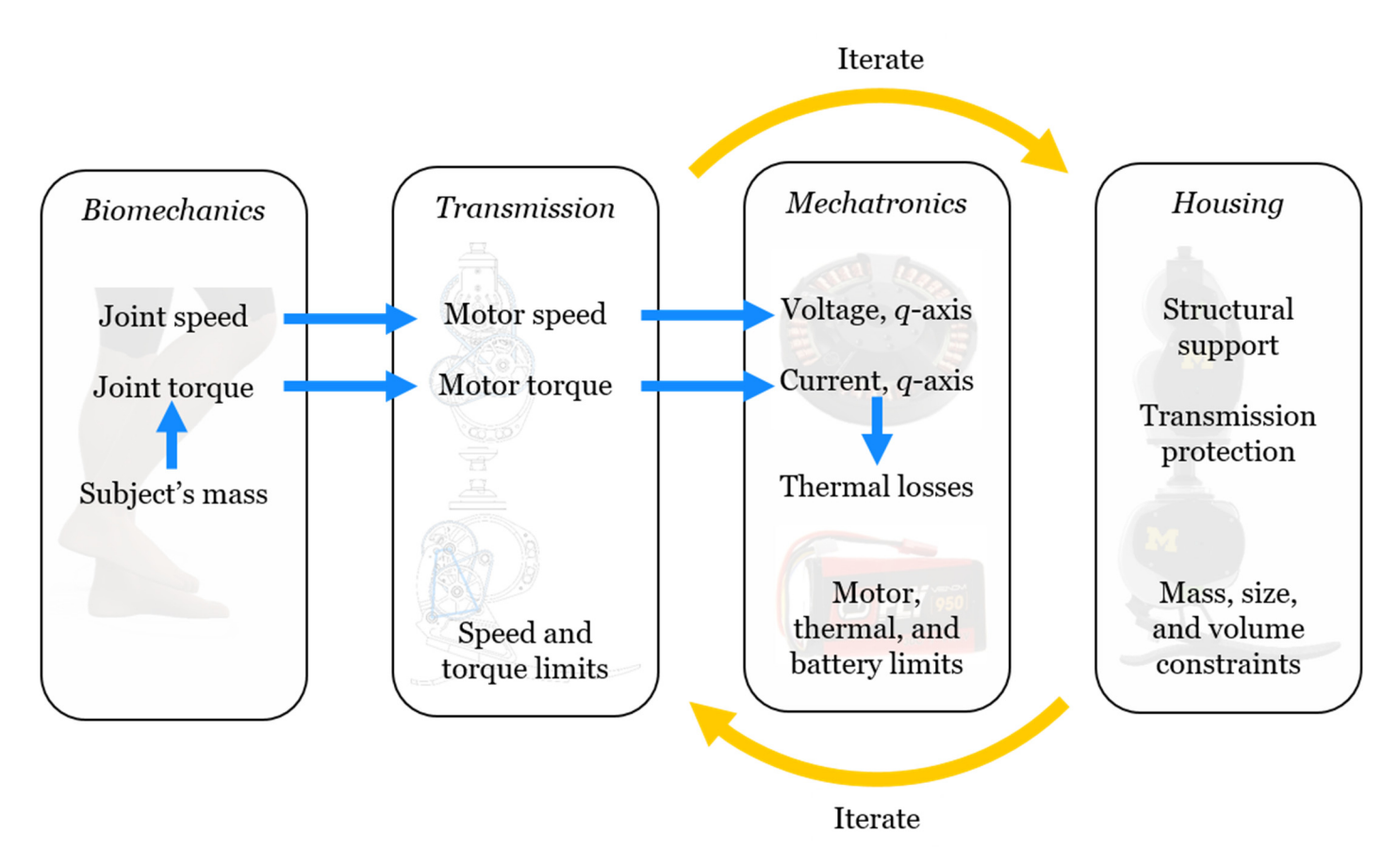


Figure 7 | **Overview of the OSL design process.** Able-bodied kinematics and kinetics provide load requirements, which are transmitted into motor kinematic (voltage) and kinetic (current) requirements. The final transmission, battery, and housing designs resulted from iterating to meet speed, torque, electrical, thermal, mass, and size constraints.

Design: biomechanics. We began the design of the OSL by extracting the kinematic (*e.g.*, angle, angular velocity, and angular acceleration) and kinetic (torque) trajectories of the knee and ankle joints from the literature. The data we used included walking at slow, self-selected, and fast speeds, in addition to stair ascent/descent, for 75 kg and 100 kg subjects⁴⁸.

Design: transmission. We simulated the transmission and motor requirements for each of the knee and ankle prostheses by incorporating the governing equations of SEAs and DC motors, and using the extracted biomechanical joint angles (θ_l) and torques (τ_l) as the desired load requirements^{22,55}. The motor mechanical requirements for a given ambulation mode are:

$$\theta_m = \left(\theta_l + \frac{\tau_l}{k_S}\right) N \tag{1}$$

$$\tau_m = J_m \ddot{\theta}_m + \frac{\tau_l}{\eta N} \tag{2}$$

where θ_m , τ_m , and J_m are motor angle, torque, and inertia, respectively; N and η are transmission ratio and efficiency (assumed $\eta = 0.9$ in each stage), respectively; and k_s is the stiffness of the series elastic element. Using equations (1) and (2), we simulated a range of transmission ratios and stiffness values (including infinite stiffness for the non-SEA configuration) for each of the ambulation modes; these simulations helped determine the range of acceptable transmission ratios and series elastic elements (Fig. S3). Based on these simulations, we selected target transmission ratios of 49:1 and 40:1-100:1 for the knee and ankle, respectively.

Timing belts serve as the primary torque transmission mechanism in the OSL; specifically, we chose the recently-developed PowerGrip GT3 (Stock Drive Products/Sterling Instrument, Hicksville, NY, USA) belts because they provide longer belt life, increased load-carrying capacity, and quieter operation relative to other available belts⁵⁶. Our overall goal when selecting belt/pulley configurations was to minimize the volume of each stage while resisting tooth jump. Tooth jump typically occurs with high torques or low belt tensioning, and is highly dependent on transmission geometry (i.e., tooth profile, number of teeth of each pulley, number of teeth engaged, pulley center-to-center distance, and belt width); however, there is little data available addressing the relationship between transmission geometry and the torque that endangers tooth jump. Based on the manufacturer's documentation, we calculated conservative estimates of tooth jump torque (per mm belt width) for 2, 3, and 5 mm pitch GT3 belts to be approximately 0.19, 0.66, and 2.4 Nm/mm, respectively⁵⁶; we used these torques to specify the minimum acceptable belt width for each transmission stage. To select the final belt drive geometries, we performed an iterative design process, investigating overall transmission volume, number of belt stages, pitch of each belt stage, width of each stage, number of teeth engaged, ease of assembly, and availability of belt lengths and widths; this process resulted in a 2 mm pitch stage followed by two 5 mm stages in the knee, and two 3 mm stages in the ankle (Table S3). These belt drives were simulated to ensure that the torques at each stage would not lead to tooth jump during ambulation (Fig. S4). The pulleys were machined from either 7075-T6 Aluminum or 17-4 PH stainless steel using subtractive manufacturing, and the belts were purchased directly from the manufacturer.

In addition to a two-stage belt drive, the ankle prosthesis incorporates a four-bar linkage mechanism for torque transmission. We included the four-bar linkage instead of a third belt stage to reduce the overall size of the prosthesis and directly couple motion of the linkage to motion of the ankle joint and foot. To design the linkage, we began by simulating the range of motion and transmission ratio of more than 3000 linkage

configurations. The simulation varied the lengths of the individual links, through integer values between 1 and 10 units, and constrained the range of motion to a minimum of 20° angular distance between links to avoid singularities (Fig. S1). Using these simulations, we explored a subset of linkage configurations while iterating through different belt drive options, and selected the mechanism that provided the best combination of range of motion, transmission ratio, and size (Fig. S1, Table S3). Increasing the range of motion of the linkage requires increasing the transmission ratio and size of the belt drive; we chose to limit the range of motion to 30° to reduce the overall size of the prosthesis. Unlike the knee, which has a constant transmission ratio, the addition of the four-bar linkage resulted in a kinematically-varying transmission ratio for the ankle (Fig. S5).

Design: mechatronics. Given the mechanical requirements in equations (1) and (2), the brushed DC electromechanical model was used to determine the electrical demands:

$$i_m = \frac{\tau_m}{k_t} \tag{3}$$

$$v_m = i_m R_m + k_b \dot{\theta}_m + L_m \frac{di_m}{dt} \tag{4}$$

where i_m , v_m , R_m , and L_m are motor current, voltage, phase resistance, and phase inductance, respectively; k_t is the torque constant; and k_b is the back-emf constant (equivalent to the magnitude of k_t in SI units). The current and voltage represent the q-axis current and voltage of field oriented control, which enables the analogy of the brushed electromechanical model. Using equations (3) and (4), we simulated various motor-battery combinations. Ultimately, the current and voltage demands (which are driven by the mechanical requirements) determined the overall mechanical design, power supply, and motor selection.

We considered multiple motors for the OSL, including the 30 mm EC-4pole motor used in the CSEA and VPL knees (model: 305015, Maxon Motor, Sachseln, Switzerland) and a high-torque, exterior rotor motor (model: U8-16, T-motor, Nanchang, Jiangxi, China) that has shown promising results in other areas of robotics^{22,31,39,57–59}. The T-motor's motor constant k_m —which describes the motor's ability to convert electrical energy to mechanical energy—is approximately 4 times higher than the EC-4pole's motor constant (Table 1); that is, the EC-4pole motor loses approximately 16 times more power than the T-motor for a given motor torque (Fig. S2). However, since the EC-4pole motors are often coupled with larger transmission ratios, they do not have to produce the same amount of torque as the T-motor. Therefore, we simulated the T-motor with the OSL knee's transmission ratio and the EC-4pole motor with the CSEA and VLP knees' transmission ratios to estimate the motors' electrical power losses within a prosthesis. After accounting for transmission ratio, the EC-4pole motor loses approximately 1.3-2 times more power to heat for a given knee torque, when compared to the T-motor (Fig. S2).

Design: housing. The OSL housing features a clamshell-style design, in which two halves are fastened together to enclose the prosthesis components (Fig. 1). The clamshell housings—machined from 7075-T6 Aluminum—serve multiple purposes: they simplify the assembly process, reduce pinch points, locate the shafts for the timing belt pulleys, and provide structural support for the OSL. The housings incorporate a system to properly tension the belt stages; appropriate belt tensioning ensures that the transmission achieves maximum torque capacity and prevents tooth jump under load. The housings also include mechanical hard stops to ensure that the OSL remains within a biomechanically-appropriate range of motion. All moving transmission components—except for the knee's proximal pyramid and the ankle's foot—are completely contained within the housing, preventing user injury and protecting the transmission from dirt and debris during testing in outdoor environments. The motors mount to the outside of the housings, allowing for convenient assembly, removal, and troubleshooting. Finally, the housings include space for batteries and electronics, creating a self-contained, portable prosthesis.

Benchtop testing. We performed several benchtop tests to quantify the OSL's performance in both the time and frequency domains. We characterized position and current controller performance through step response and bandwidth tests, and tested the thermal response of the motor and prosthesis given a constant current input. A testing rig mechanically grounded the knee and ankle joints—and provided a reaction torque—during the current control tests; during the position control tests, the joints were free to rotate (Fig. S6). For these benchtop tests, we used a single-board computer (Table S1) to send the desired current and position trajectories (via USB at approximately 750 Hz) to the Dephy actuator, which subsequently performed lowlevel feedback control (Fig. 2). We tested the knee and ankle separately, and did not test with series elasticity.

463

464

465

466

467

468

469 470

471

472

473

476

477

478

479

480 481

482

483

484

485

486

487

488 489

490

491

492 493

494

495

496

497

498

499

500

501

502

503

504

505

506

We quantified the OSL's ability to track desired position and current commands by conducting step response tests (Fig. 3). We commanded motor encoder steps corresponding to 5°, 10°, and 15° steps at the joint, starting from the midpoint of the range of motion; we also commanded current steps of 2 A, 4 A, and 6 A (peak phase current), corresponding to 0.8 A, 1.5 A, and 2.3 A of q-axis current, respectively. We performed 5 trials for 474 475 each condition.

To quantify the range of frequencies in which the OSL can track position and current commands, we performed frequency response tests (Fig. 3). The position trajectories were Gaussian white noise signals—3rd order, 40 Hz low-pass filtered—scaled to ± 5°, 10°, and 15° amplitudes, and centered at the midpoint of the range of motion; the current trajectories were also Gaussian white noise signals—3rd order, 200 Hz low-pass filtered—scaled to \pm 0.8 A, 1.5 A, and 2.3 A amplitudes, and centered at 0 A. The position trials lasted for 15 s whereas the current trials lasted for 60 s. We conducted 5 trials for each condition and constructed Bode plots using Blackman-Tukey spectral analysis, where the auto-spectrum and cross-spectrum are divided in the frequency domain⁶⁰. Using the Bode plots, we calculated bandwidth as the frequency in which the magnitude crossed -3 dB.

Although we did not use series elasticity in the benchtop and amputee experiments, we did characterize the stiffness of the elastic elements when included inside the knee output pulley (Fig. 1). We mounted the knee onto a six-axis load sensor (model: 45E15A4, JR3, Inc., Woodland, CA, USA) and manually rotated the knee from 0° to 15° and back. We performed 5 trials each for the following configurations: 0, 1, 2, 3, 4, 5, and 6 springs. We also locked the input shaft to ensure that the knee's rotation was due to spring deflection instead of belt drive motion.

To test the thermal behavior of the OSL we supplied the motor with a constant current of 8 A across two winding leads for 70 minutes using a power supply (model: 1688B, B&K Precision Corp., Yorba Linda, CA, USA), and measured the resulting change in winding and housing temperature using a thermal imaging camera (model: ONE Pro LT, FLIR Systems, Inc., Wilsonville, OR, USA). The T-motor is delta wound, meaning when current is supplied between two leads, one phase has twice the current of the other two phases (Fig. 3). Consequently, we estimated winding temperature as the weighted average of the more and less powered windings. We subsequently modeled the thermal dynamics of the motor by simulating the equivalent electrical circuit (Fig. 3) in Simulink^{33,61}. In this model, temperature and heat flow are analogous to voltage and current, respectively; heat flow is equivalent to the thermal power lost (P_{loss}) through the electrical resistance of the motor, which is a function of temperature:

$$P_{loss} = i_m^2 R_m = i_m^2 R_{m,A} (1 + \alpha_{Cu} (T_w - T_A))$$
(7)

where $R_{m,A}$ is the motor electrical resistance at ambient (room) temperature, α_{Cu} is copper's temperature coefficient of resistance, and T_w and T_A are winding and ambient temperature, respectively. We used the measured temperature data to calculate the motor's optimal thermal parameters: winding-housing thermal resistance and capacitance ($R_{th,w}$ and $C_{th,w}$), as well as housing-ambient thermal resistance and capacitance $(R_{th,h} \text{ and } C_{th,h}).$

507 Clinical testing. To test the OSL's capability to restore gait, and demonstrate control implementation on the hardware platform, we used a previously-developed control approach³⁸. We implemented locomotion 508 controllers for standing, level-ground walking, ramp ascent/descent, and stair ascent/descent using impedance 509 510 control; the impedance parameters for each ambulation mode regulate the current to the knee and ankle motors based on the desired torque⁶². Within our tuning process, a finite state-machine divides all gait 511 activities (except for standing) into four sub-phases: early-to-mid stance, late stance, swing flexion, and swing 512 extension; simple logic based on mechanical sensors within the prosthesis (e.g., joint encoders, load sensor, 513 514 etc.) enabled progression through the state-machine. The standing mode controller only uses two states; the first is relatively stiff to support the weight of the body when the prosthesis is in contact with the ground, and 515 the second allows the leg to swing freely when it is not in contact with the ground. The desired motor current 516 is determined by converting the desired joint torque τ_i , into motor current: 517

$$\tau_j = -k_j (\theta_j - \theta_{0j}) - b_j \dot{\theta}_j \tag{8}$$

where j corresponds to the knee or ankle joint, θ is joint angle (positive values represent knee extension and ankle dorsiflexion), and $\dot{\theta}$ is joint angular velocity. The three tunable impedance parameters for each joint are virtual stiffness k, virtual equilibrium angle θ_0 , and virtual damping coefficient b. The desired joint torque is converted to desired motor torque using the transmission ratio, and desired motor current is calculated using equation (3).

For 60% of the states (across all ambulation modes), we hold impedance parameters at tuned, but constant values; for the remaining 40% of the states, we modulate the impedance parameters according to the following five control laws: (1) basing impedance parameters on values from the previous state; (2) mimicking biological joint responses (*i.e.*, modifying joint impedance as a function of ankle angle); (3) modifying joint impedance as a function of knee angle; or allowing users to control the rate of power generation/dissipation (*i.e.*, modifying joint impedance as a function of (4) decreasing or (5) increasing prosthesis load). We discuss each of these approaches in detail in our previous work³⁸; these control strategies are used to reduce the number of independent parameters required to tune the prosthesis and improve transitions between different types of activities. This control scheme creates an overall system response that allows each subject to walk safely, comfortably, and confidently. For these clinical tests, we used an embedded microcontroller (Table S1) to perform high-level control (at approximately 40 Hz) and send the desired current trajectories to the DAP, which subsequently performed low-level feedback control; the microcontroller and DAP communicated via SPI (Fig. 2).

References and Notes

518

524

525526

527

528

529

530

531532

533

534535

536

537

538

539

540

- 1. Ziegler-Graham, K., MacKenzie, E. J., Ephraim, P. L., Travison, T. G. & Brookmeyer, R. Estimating the Prevalence of Limb Loss in the United States: 2005 to 2050. *Arch. Phys. Med. Rehabil.* **89**, 422–429 (2008).
- 541 2. Sinha, R., Van Den Heuvel, W. J. A. & Arokiasamy, P. Factors affecting quality of life in lower limb amputees. *Prosthet. Orthot. Int.* **35**, 90–96 (2011).
- Waters, R. L., Perry, J., Antonelli, D. & Hislop, H. Energy cost of walking of amputees: the influence of level of amputation. *J. Bone Joint Surg. Am.* **58**, 42–46 (1976).
 - 4. Au, S. K. & Herr, H. M. Powered ankle-foot prosthesis. *IEEE Robot. Autom. Mag.* 15, 52–59 (2008).
- 546 5. Miller, W. C., Speechley, M. & Deathe, B. The prevalence and risk factors of falling and fear of falling among lower extremity amputees. *Arch. Phys. Med. Rehabil.* **82**, 1031–1037 (2001).
- 548 6. Winter, D. A. *Biomechanics and Motor Control of Human Movement*. (Wiley, 2009). doi:10.1002/9780470549148
- Harvey, Z. T., Potter, B. K., Vandersea, J. & Wolf, E. Prosthetic advances. J. Surg. Orthop. Adv. 21,

551 58–64 (2012).

- Nolan, L. *et al.* Adjustments in gait symmetry with walking speed in trans-femoral and trans-tibial amputees. *Gait Posture* **17**, 142–151 (2003).
- Winter, D. A. & Sienko, S. E. Biomechanics of below-knee amputee gait. *J. Biomech.* **21**, 361–367 (1988).
- 556 10. Gailey, R., Allen, K., Castles, J., Kucharik, J. & Roeder, M. Review of secondary physical conditions 557 associated with lower-limb amputation and long-term prosthesis use. *J. Rehabil. Res. Dev.* **45**, 15–29 558 (2008).
- 559 11. Rybarczyk, B. *et al.* Social discomfort and depression in a sample of adults with leg amputations. *Arch. Phys. Med. Rehabil.* **73**, 1169–1173 (1992).
 - 12. Murray, C. D. The Social Meanings of Prosthesis Use. *J. Health Psychol.* **10**, 425–441 (2005).
- 562 13. Cherelle, P., Mathijssen, G., Wang, Q., Vanderborght, B. & Lefeber, D. Advances in Propulsive Bionic 563 Feet and Their Actuation Principles. *Adv. Mech. Eng.* **2014**, 1–21 (2014).
- Windrich, M., Grimmer, M., Christ, O., Rinderknecht, S. & Beckerle, P. Active lower limb prosthetics: a systematic review of design issues and solutions. *Biomed. Eng. Online* **15**, 5–19 (2016).
- Lara-Barrios, C. M., Blanco-Ortega, A., Guzmán-Valdivia, C. H. & Bustamante Valles, K. D. Literature review and current trends on transfemoral powered prosthetics. *Adv. Robot.* **32**, 51–62 (2018).
- 569 16. Quintero, D., Villarreal, D. J. & Gregg, R. D. Preliminary Experiments with a Unified Controller for a 570 Powered Knee-Ankle Prosthetic Leg Across Walking Speeds. *IEEE Int. Conf. Intell. Robot. Syst.* 571 (2016).
- 572 17. Quintero, D. *et al.* Continuous-Phase Control of a Powered Knee Ankle Prosthesis: Amputee Experiments Across Speeds and Inclines. *IEEE Trans. Robot.* **34**, 686–701 (2018).
- Thatte, N. & Geyer, H. Toward balance recovery with leg prostheses using neuromuscular model control. *IEEE Trans. Biomed. Eng.* **63**, 904–913 (2016).
- 576 19. Liu, M., Zhang, F., Datseris, P. & Huang, H. Improving Finite State Impedance Control of Active-577 Transfemoral Prosthesis Using Dempster-Shafer Based State Transition Rules. *J. Intell. Robot. Syst.* 578 *Theory Appl.* **76**, 461–474 (2014).
- Zhao, H., Horn, J., Reher, J., Paredes, V. & Ames, A. D. Multicontact Locomotion on Transfemoral
 Prostheses via Hybrid System Models and Optimization-Based Control. *IEEE Trans. Autom. Sci. Eng.* 13, 502–513 (2016).
- 582 21. Clites, T. R. *et al.* Proprioception from a neurally controlled lower-extremity prosthesis. *Sci. Transl.* 583 *Med* **10**, (2018).
- Rouse, E. J., Mooney, L. M. & Herr, H. M. Clutchable series-elastic actuator: Implications for prosthetic knee design. *Int. J. Robot. Res.* **33**, 1611–1625 (2014).
- Pfeifer, S., Pagel, A., Riener, R. & Vallery, H. Actuator with angle-dependent elasticity for biomimetic transfemoral prostheses. *IEEE/ASME Trans. Mechatronics* **20**, 1384–1394 (2015).
- 588 24. Gard, S. A. & Childress, D. S. What Determines the Vertical Displacement of the Body during Normal Walking? *J. Prosthetics Orthot.* **13**, 64–67 (2001).
- 590 25. Segal, A. D. *et al.* Kinematic and kinetic comparisons of transfemoral amputee gait using C-Leg ® and Mauch SNS ® prosthetic knees. **43**, 857–870 (2006).
- Au, S. K., Weber, J. & Herr, H. M. Powered ankle-foot prosthesis improves walking metabolic economy. *IEEE Trans. Robot.* **25**, 51–66 (2009).
- Hitt, J. K., Sugar, T. G., Holgate, M. & Bellman, R. An Active Foot-Ankle Prosthesis With Biomechanical Energy Regeneration. *J. Med. Device.* **4**, 011003 (2010).
- 596 28. Cherelle, P., Grosu, V., Matthys, A., Vanderborght, B. & Lefeber, D. Design and validation of the

- ankle mimicking prosthetic (AMP-) Foot 2.0. *IEEE Trans. Neural Syst. Rehabil. Eng.* **22**, 138–148 (2014).
- Wang, Q., Yuan, K., Zhu, J. & Wang, L. Walk the walk: A lightweight active transtibial prosthesis. *IEEE Robot. Autom. Mag.* **22**, 80–89 (2015).
- Gardinier, E. S., Kelly, B. M., Wensman, J. & Gates, D. H. A controlled clinical trial of a clinicallytuned powered ankle prosthesis in people with transtibial amputation. *Clin. Rehabil.* 026921551772305 (2017). doi:10.1177/0269215517723054
- Lawson, B. E. *et al.* A robotic leg prosthesis: Design, control, and implementation. *IEEE Robot. Autom. Mag.* **21**, 70–81 (2014).
 - 32. Cempini, M., Hargrove, L. J. & Lenzi, T. Design, development, and bench-top testing of a powered polycentric ankle prosthesis. *IEEE Int. Conf. Intell. Robot. Syst.* **2017-Septe**, 1064–1069 (2017).
 - 33. Lenzi, T., Cempini, M., Hargrove, L. J. & Kuiken, T. A. Design, Development, and Testing of a Lightweight Hybrid Robotic Knee Prosthesis. *Int. J. Rob. Res.* in press, (2018).

607

608

- 610 34. Caputo, J. M. & Collins, S. H. A universal ankle-foot prosthesis emulator for human locomotion experiments. *J. Biomech. Eng.* **136**, 035002 (2014).
- Kim, M., Chen, T., Chen, T. & Collins, S. H. An Ankle–Foot Prosthesis Emulator With Control of Plantarflexion and Inversion–Eversion Torque. *IEEE Trans. Robot.* In Press, 1–12 (2018).
- Tucker, M. R. *et al.* Control Strategies for Active Lower Extremity Prosthetics and Orthotics: A Review. *J. Neuroeng. Rehabil.* (2015). doi:10.1186/1743-0003-12-1
- Hargrove, L. J. *et al.* Intuitive control of a powered prosthetic leg during ambulation: a randomized clinical trial. *J. Am. Med. Assoc.* **313**, 2244–52 (2015).
- Simon, A. M. *et al.* Configuring a powered knee and ankle prosthesis for transfemoral amputees within five specific ambulation modes. *PLoS One* **9**, (2014).
- Wang, S. *et al.* Design and Control of the MINDWALKER Exoskeleton. *IEEE Trans. Neural Syst. Rehabil. Eng.* **23**, 277–286 (2015).
- 40. Pratt, G. A. & Williamson, M. M. Series Elastic Actuators. in *IEEE/RSJ International Conference on Intelligent Robots and Systems* 399–406 (1995).
- Duval, J. F. & Herr, H. M. FlexSEA: Flexible, Scalable Electronics Architecture for wearable robotic applications. *Proc. IEEE RAS EMBS Int. Conf. Biomed. Robot. Biomechatronics* 1236–1241 (2016). doi:10.1109/BIOROB.2016.7523800
- Duval, J. F. & Herr, H. M. FlexSEA-Execute: Advanced motion controller for wearable robotic
 applications. *Proc. IEEE RAS EMBS Int. Conf. Biomed. Robot. Biomechatronics* 1056–1061 (2016).
 doi:10.1109/BIOROB.2016.7523771
- Azocar, A. F., Mooney, L. M., Hargrove, L. J. & Rouse, E. J. Design and Characterization of an Open-source Robotic Leg Prosthesis. in *IEEE International Conference on Biomedical Robotics and Biomechatronics* 111–118 (2018).
- Lee, U. H., Pan, C. & Rouse, E. J. Empirical Characterization of a High-performance Exterior-rotor Type Brushless DC Motor and Drive. in *IEEE Int. Conf. on Intelligent Robots and Systems* (2019).
- Hargrove, L. J. *et al.* Robotic leg control with EMG decoding in an amputee with nerve transfers. *N. Engl. J. Med.* **369**, 1237–42 (2013).
- 46. Young, A. J., Simon, A. M. & Hargrove, L. J. A training method for locomotion mode prediction using powered lower limb prostheses. *IEEE Trans. Neural Syst. Rehabil. Eng.* **22**, 671–677 (2014).
- 639 47. Tilley, A. R. The Measure of Man and Woman: Human Factors in Design. (Watson-Guptill, 1993).
- 8. Bovi, G., Rabuffetti, M., Mazzoleni, P. & Ferrarin, M. A multiple-task gait analysis approach:
- kinematic, kinetic and EMG reference data for healthy young and adult subjects. *Gait Posture* **33**, 6–13 (2011).

- 49. McIntosh, A. S., Beatty, K. T., Dwan, L. N. & Vickers, D. R. Gait dynamics on an inclined walkway. *J. Biomech.* 39, 2491–2502 (2006).
- 645 50. Protopapadaki, A., Drechsler, W. I., Cramp, M. C., Coutts, F. J. & Scott, O. M. Hip, knee, ankle 646 kinematics and kinetics during stair ascent and descent in healthy young individuals. *Clin. Biomech.* 22, 647 203–210 (2007).
- 51. Stepien, J. M., Cavenett, S., Taylor, L. & Crotty, M. Activity Levels Among Lower-Limb Amputees: Self-Report Versus Step Activity Monitor. *Arch. Phys. Med. Rehabil.* **88**, 896–900 (2007).
- Tudor-Locke, C. & Bassett, D. How many steps/day are enough? Preliminary pedometer indicies for public health. *Sport. Med.* **34**, 1–8 (2004).
 - 53. Browning, R. C., Modica, J. R., Kram, R. & Goswami, A. The effects of adding mass to the legs on the energetics and biomechanics of walking. *Med. Sci. Sports Exerc.* **39**, 515–525 (2007).
 - 54. Schmalz, T., Blumentritt, S. & Marx, B. Biomechanical analysis of stair ambulation in lower limb amputees. *Gait Posture* **25**, 267–278 (2007).
 - 55. Lynch, K. M., Marchuk, N. & Elwin, M. *Embedded Computing and Mechatronics with the PIC32 Microcontroller*. (Newnes, 2016).
 - 56. Stock Drive Products/Sterling Instrument (SDP/SI). *Handbook of Timing Belts, Pulleys, Chains and Sprockets*.
- Kalouche, S. GOAT: A Legged Robot with 3D Agility and Virtual Compliance. in *Intelligent Robots and Systems (IROS), 2017 IEEE/RSJ International Conference* 4110–4117 (2017).
 - 58. Kenneally, G., De, A. & Koditschek, D. E. Design Principles for a Family of Direct-Drive Legged Robots. *IEEE Robot. Autom. Lett.* **1**, 900–907 (2016).
 - 59. Seok, S. *et al.* Design Principles for Energy-Efficient Legged Locomotion and Implementation on the MIT Cheetah Robot. *IEEE/ASME Trans. Mechatronics* **20**, 1117–1129 (2015).
 - 60. Ljung, L. System Identification: Theory for the User. (Prentice Hall PTR, 1999).
 - 61. Braun, J. Formulae Handbook. (2012).
- 668 62. Sup, F., Varol, H. A. & Goldfarb, M. Upslope walking with a powered knee and ankle prosthesis: Initial results with an amputee subject. *IEEE Trans. Neural Syst. Rehabil. Eng.* **19**, 71–78 (2011).

Acknowledgments

652

653

654

655

656

657658

659

662

663

664

665

666

667

670671672

673

674675

676677

678

679

680 681

682

683

684 685

686

687

688

689

Acknowledgements: This work was supported by the National Science Foundation (NSF) Graduate Research Fellowship under Grant No. DGE-1324585, NSF National Robotics Initiative (NRI) under Grant No. CMMI 1734586, and the MSL Renewed Hope Foundation. The authors would like to thank U. H. Lee, T. Sharkey, and M. Mongeon for their assistance.

Author contributions: AFA, LMM, and EJR developed the prosthesis. LMM and JFD developed the Dephy Actuator Package. AFA performed the benchtop experiments. AMS and LJH performed the clinical experiments. AFA analyzed the data with input from EJR. AFA and EJR wrote the manuscript, with input from LMM, JFD, AMS, and LJH. All authors approved of the final version.

Competing interests: LMM and JFD are co-founders of Dephy, Inc., who supports the open-source FlexSEA project, as well as its proprietary, commercial derivatives.

Data and code availability: The clinical data that support the findings of this study are available as supplementary information files, and hosted on the website for the Open Source Bionic Leg project (www.opensourceleg.com). Solid model files, bill of materials, links to suppliers, control system code, instructional guides, and videos on assembly/disassembly are available on the website.

Supplementary Materials

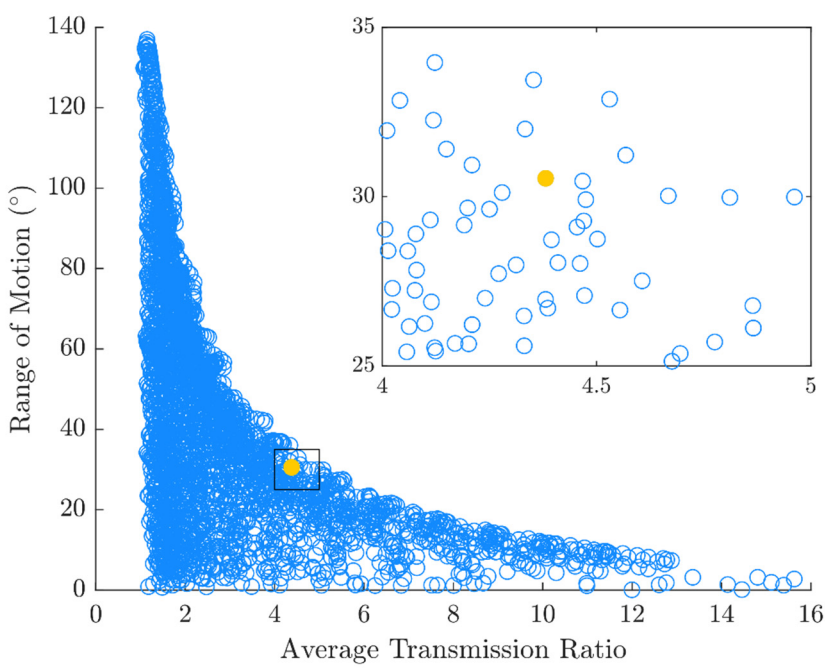


Figure S1 | Simulated range of motion and transmission ratio for various linkage configurations. Design of the linkage required a tradeoff between ankle range of motion and transmission ratio. Filled yellow circle denotes the linkage implemented in the ankle prosthesis.

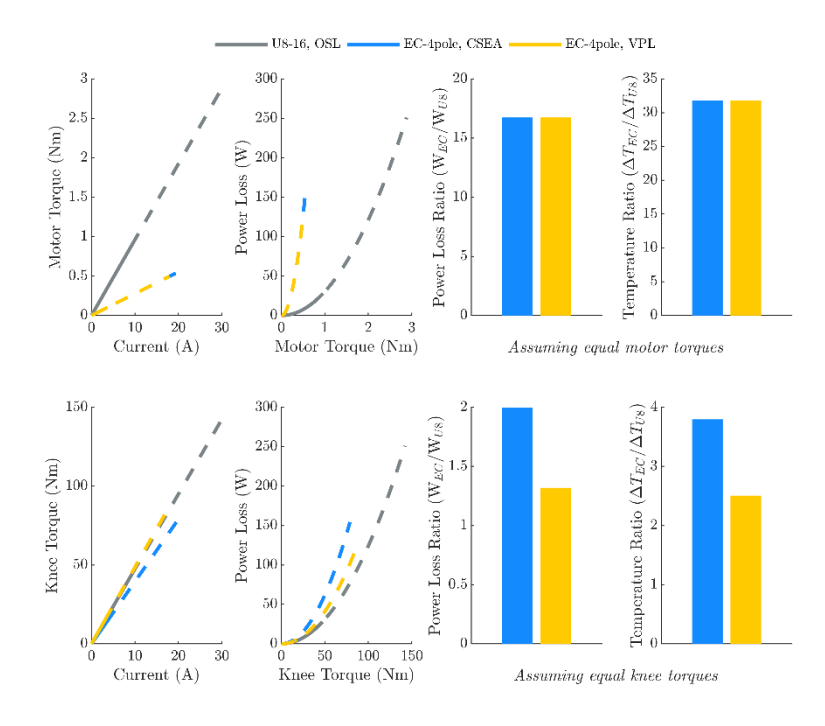


Figure S2 | **Motor and prosthesis efficiency comparison.** Comparison of the (top) T-motor and Maxon motor used in the CSEA and VPL, and of the (bottom) motors coupled to the transmission ratio used in their respective prostheses. **a**, Torque-current relationship. **b**, Electrical power loss (i^2R) as a function of torque, assuming zero angular velocity. **c**, Ratio of the EC-4pole motor's power loss to the

 $\begin{array}{c} 711 \\ 712 \end{array}$

U8-16 motor's power loss. **d**, Ratio of the EC-4pole motor's temperature increase to the U8-16 motor's temperature increase.

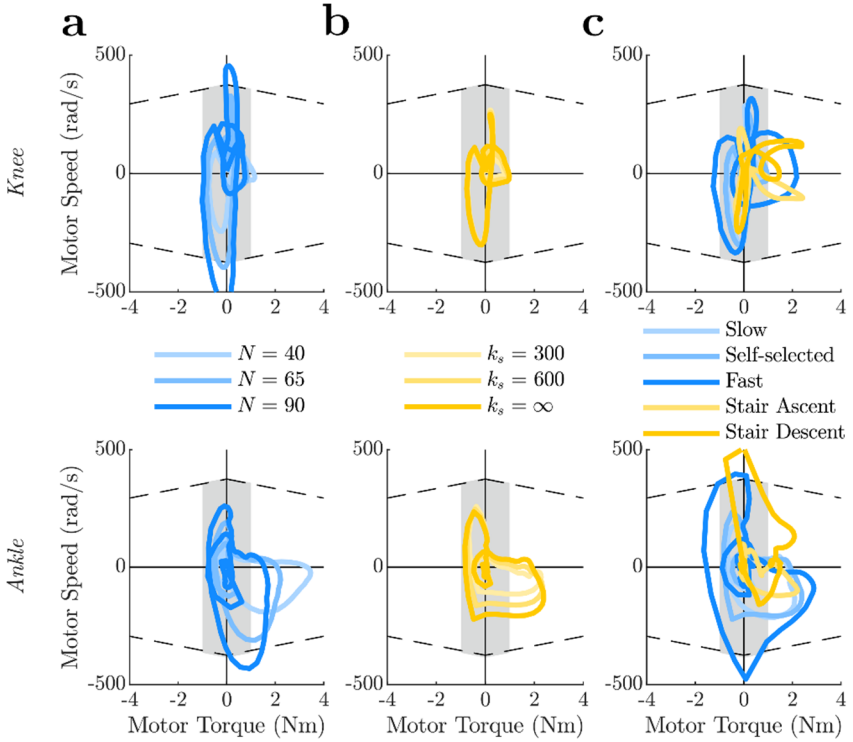


Figure S3 | Simulated motor speed-torque curves for the knee and ankle prostheses. a, Transmission ratio simulation in a non-SEA configuration for self-selected walking. b, SEA simulation with the OSL transmission ratios for self-selected walking. c, Ambulation mode simulation in a non-SEA configuration using the OSL transmission ratios. Shaded area denotes the continuous operating region.

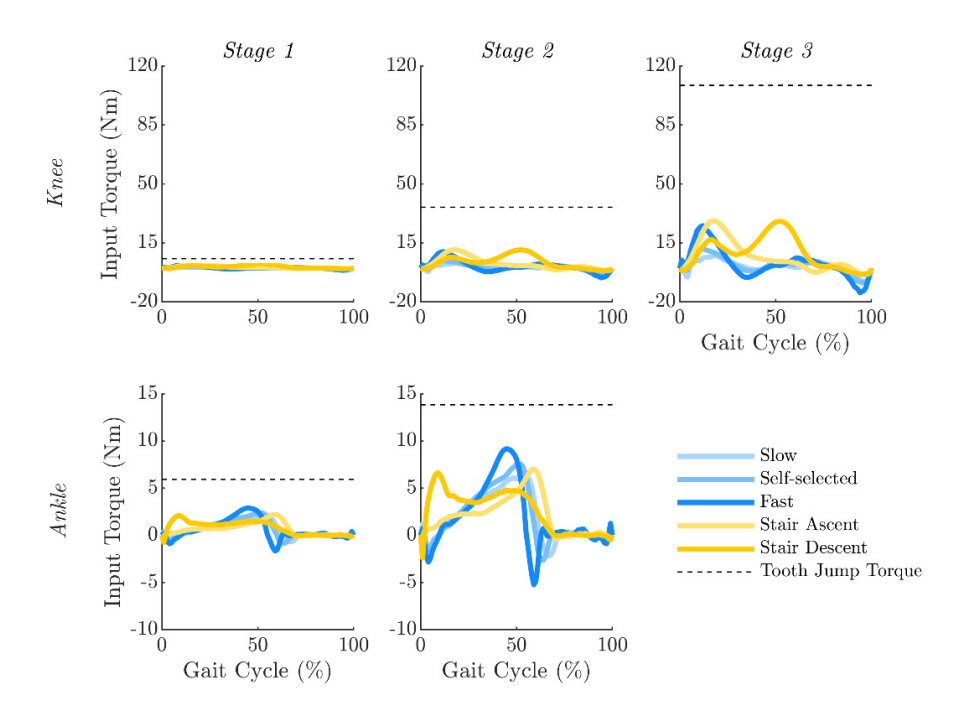


Figure S4 | Simulated belt drive torques for the knee and ankle prostheses. The expected torques applied to the input pulleys of the belt drive stages are below the tooth jump torque across all the simulated ambulation modes.

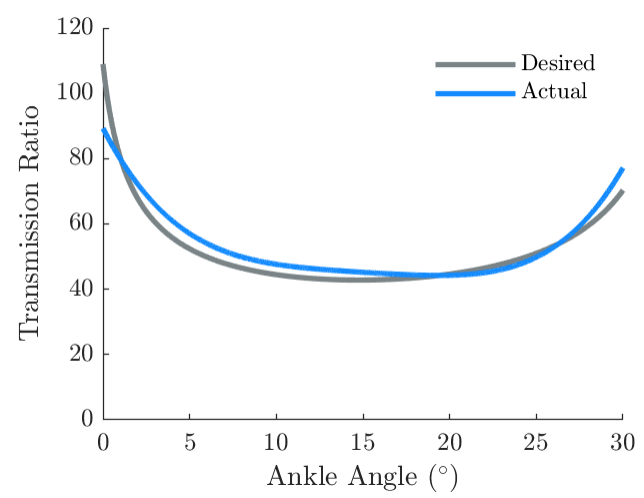


Figure S5 | Ankle transmission ratio throughout the range of motion.

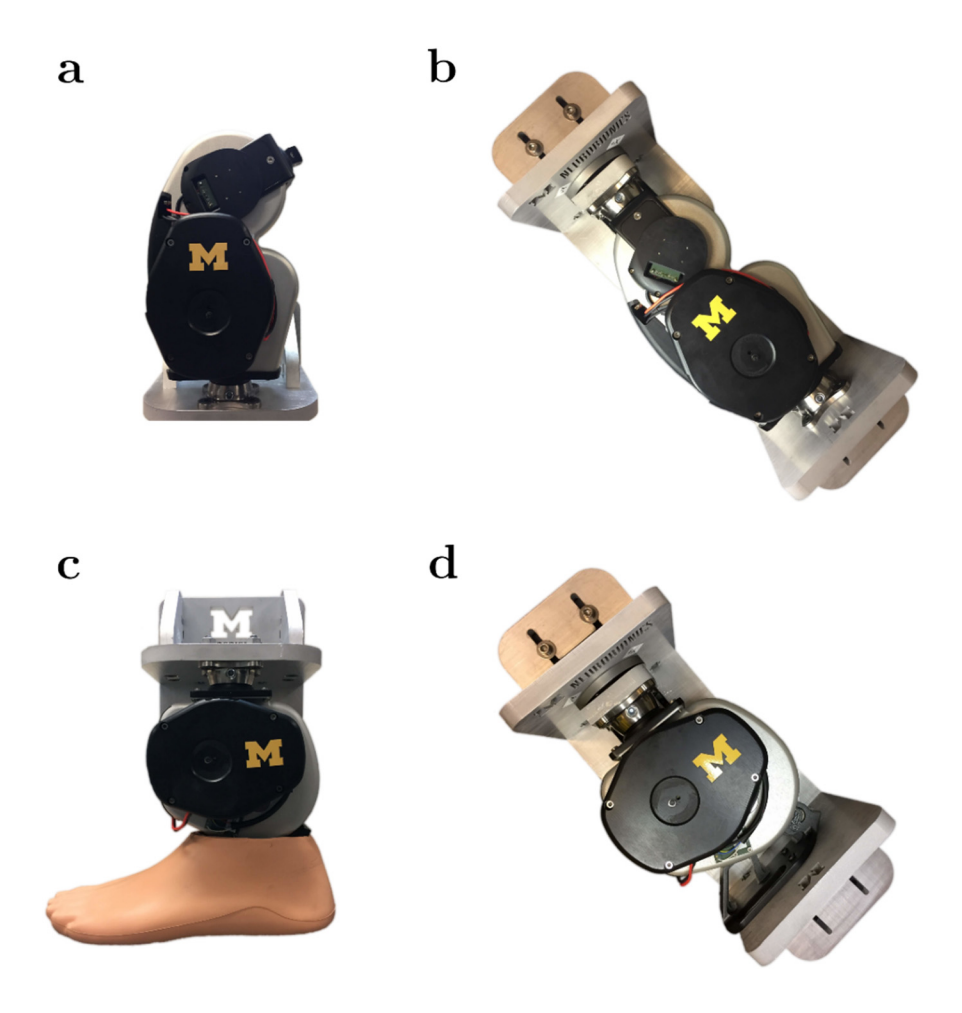


Figure S6 | Benchtop testing setup. a, Knee position controller testing—knee joint is free to rotate. b, Knee current controller and thermal response testing. c, Ankle position controller testing—ankle joint is free to rotate. d, Ankle current controller testing.

Table S1 | Hardware model information.

Item	Model	Company	Location
Motor	U8-16	T-motor	Nanchang, Jiangxi, China
Batteries	25087X2	Venom Power	Rathdrum, ID, USA
Temperature Sensor	MCP9700A	Microchip Technology Inc.	Chandler, AZ, USA
IMU	MPU-9250	InvenSense	San Jose, CA, USA
Motor Encoder	AS5047P	ams AG	Premstaetten, Austria
Joint Encoder	AK7452	Asahi Kasei Microdevices Corporation	Tokyo, Japan
Load Sensor	M3564F	Sunrise Instruments	Nanning, China
Single-board Computer	Raspberry Pi 3	Raspberry Pi Foundation	Cambridge, UK
Embedded Microcontroller	DM3730	Texas Instruments	Dallas, TX, USA

Table S2 | Subject characteristics.

Subject	Gender	Age (years)	Time Post- amputation (years)	Etiology	Weight (kg)	Height (m)	Mobility Level	Prescribed Knee Prosthesis
TF1	F	51	29	Traumatic	61.7	1.65	K3	Rheo
TF2	M	33	2	Sarcoma	63.1	1.77	К3	Genium
TF3	M	70	44	Traumatic	86.2	1.75	К3	C-Leg

Table S3 | Transmission specifications.

		Knee				Ankle			
		Stage 1	Stage 2	Stage 3	Stage 1	Stage 2	Stage 3		
Belt Drive	Pitch (mm)	2	5	5	3	3	-		
	Input Pulley Teeth	16	14	14	17	17	-		
	Output Pulley Teeth	80	40	48	60	60	-		
	Transmission Ratio	5.00	2.86	3.43	3.53	3.53	-		
	Belt Teeth	92	50	60	72	72	-		
	Belt Width (mm)	30	15	45	9	21	-		
Linkage	Crank Length (mm)	-	-	-	-	-	2		
	Coupler Length (mm)	-	-	-	-	-	10		
	Rocker Length (mm)	-	-	-	-	-	7		
	Frame Length (mm)	-	-	-	-	-	10		
	Transmission Ratio	-	-	-	-	-	3.44-8.75		
	Range of Motion (°)	-	-	-	-	-	30.54		

744	Movie S1 Thermal response to a constant current input of 8 A DC across two winding leads.